IAES International Journal of Robotics and Automation (IJRA)
Vol. 15, No. 4, December 2026, pp. 779~797
ISSN: 2722-2586, DOI: 10.11591/ijra.v15i4.pp779-797

Design and evaluation of an IoT-enabled mobile medical supply carrier with vital-sign monitoring and video streaming

Henry Candra[1], Umi Yuniati[1], Tjhwa Endang Djuana[1], Indra Surjati[2], Raden Deiny Mardian Wijayapraja[1], Syah Alam[1], Yuli Kurnia Ningsih[1], Lydia Sari[1], Rifai Chai[3], Angellia Lestari Candra[4]
[1]Master of Electrical Engineering, Faculty of Industrial Technology, Universitas Trisakti, Jakarta, Indonesia
[2]Professional Program for Engineers, Faculty of Industrial Technology, Universitas Trisakti, Jakarta, Indonesia
[3]School of Engineering, Swinburne University of Technology, Melbourne, Australia
[4]Electrical Engineering Department, Faculty of Industrial Technology, Universitas Trisakti, Jakarta, Indonesia

Article Info

Article history:

Received Jan 30, 2026
Revised Aug 24, 2026
Accepted Nov 10, 2026

Keywords:

Healthcare automation
Internet of Things
Mobile medical logistics
Video streaming
Vital-sign monitoring

ABSTRACT

Hospitals require internal logistics systems that reduce unnecessary physical contact while maintaining remote observation and basic patient-support functions. This paper presents an applied robotics prototype of a low-cost IoT-enabled mobile medical supply carrier that uniquely integrates multiple functions in one compact platform: payload transport, ESP32-CAM telepresence, MLX90614 non-contact temperature sensing, MAX30100 pulse-oximetry monitoring, and an optional Kinect-based human-in-the-loop gesture interface. Unlike single-function delivery or monitoring devices, the prototype is evaluated as an integrated healthcare-support robot with sensing, teleoperation, video feedback, and supervised interaction. The system uses an ESP32 controller, differential-drive mobile base, Wi-Fi dashboard, camera module, and compact sensing modules. Experiments evaluated temperature accuracy, payload-speed behavior, video-streaming feasibility, Kinect tracking responsiveness, continuous-operation reliability, and practical command/video latency to define the system operating envelope. The MLX90614 achieved the lowest temperature error at 1 cm (0.84%) but increased to 22.66% at 3 cm. The carrier transported payloads up to 2.098 kg at reduced speed (0.091 m/s), while motion failed at 2.445 kg. The MAX30100 produced average errors of 1.13% for SpO2 and 6.92% for pulse rate. Kinect tracking was reliable at 120-420 cm with 49-187 ms sample gaps, and additional observations confirmed stable 30-min teleoperation with practical command-response latency below 110 ms.

This is an open access article under the CC BY-SA license.

Corresponding Author:

Henry Candra
Master of Electrical Engineering, Faculty of Industrial Technology, Universitas Trisakti
Jakarta, Indonesia
Email: henrycandra@trisakti.ac.id

1. INTRODUCTION

Robotics and internet-of-things (IoT) technologies are increasingly used to support healthcare automation, particularly for repetitive logistics, remote observation, and contact-reduction tasks in infection-sensitive environments. Hospital-support logistics require frequent short-range transport of medicines, consumables, and small instruments, while healthcare workers must still maintain awareness of the patient and device condition. Recent healthcare robotics studies report growing use of robots for assistance, telepresence, monitoring, and service-support tasks, but their deployment remains heterogeneous in technical scope, usability, and operational readiness [1]–[5]. Telepresence and assistive robotic platforms have also been investigated in primary care, emergency departments, isolation-related workflows, and broader human-

robot interaction contexts, where remote presence and safe mobility can improve service continuity and reduce direct physical contact [6]–[8].

Hospital-support robots have evolved from delivery-oriented mobile bases and telepresence systems toward more integrated platforms that combine mobility, sensing, and operator interaction. However, the remaining gap is not the absence of hospital robots or IoT monitoring systems as separate technologies, but the limited experimental evaluation of compact low-cost prototypes that combine logistics transport, live video-based telepresence, and basic physiological monitoring in one mobile carrier. Recent gesture-driven and immersive teleoperation studies further indicate that human-in-the-loop control is becoming more practical for mobile robots, including healthcare-oriented environments [9], [10]. Therefore, an integrated prototype must be evaluated not only as a transport device, but also as a teleoperated robotic system with sensing, video feedback, user interaction, and safety-aware operating constraints [1], [3], [5], [6].

Accordingly, this work aims to design and evaluate an IoT-enabled mobile medical supply carrier prototype that integrates payload transport, non-contact temperature sensing, pulse-oximetry-based monitoring, ESP32-CAM video streaming, and an optional Kinect-based gesture interface for human-in-the-loop teleoperation. The main novelty is the functional combination and evaluation of healthcare logistics, telepresence, vital-sign monitoring, and gesture-based supervisory control in a single low-cost applied robotics platform rather than as isolated modules. This positioning differentiates the proposed prototype from conventional single-function hospital delivery robots or standalone monitoring systems.

The specific objectives are to: i) develop a compact hardware-software architecture that unifies delivery, video feedback, and basic sensing; ii) quantify feasibility through temperature-sensing, pulse-oximetry, payload-speed, video-streaming, and Kinect responsiveness tests; iii) characterize short-duration reliability and practical command/video latency under indoor Wi-Fi conditions; and iv) identify realistic operating boundaries and future engineering requirements for supervised hospital-support deployment.

2. RELATED WORK

Recent hospital and service-robot studies show that mobile platforms can support healthcare logistics, patient assistance, and infection-sensitive workflows. Pranathi *et al.* [11] presented a patient-assistance robot for routine support tasks, while Haider *et al.* [12] focused on robotic assistance for isolated COVID-19 patients. Hasan *et al.* [13] also emphasized the development of a cost-effective assistive robot. These studies demonstrate the feasibility of low-cost robotic support in healthcare environments; however, their main emphasis is assistance or pandemic-response functionality rather than the combined evaluation of payload transport, telepresence video, and embedded vital-sign monitoring in a single mobile prototype.

Hospital delivery and navigation-oriented platforms provide a second relevant line of work. Antony *et al.* [14] reported an automatic guided vehicle for hospital applications, and Chien *et al.* [15] investigated service-robot navigation in complex indoor environments. Narayanan *et al.* [16] proposed a wireless-guided nursing robot, while Rusdi *et al.* [17] developed an IoT-based patient-service robot. Ward-delivery simulation and infection-reduction studies further confirm the value of robotic support for internal hospital logistics [18], [19]. Nevertheless, many of these works mainly emphasize navigation, service delivery, or infection-risk reduction, with limited experimental attention to the simultaneous integration of telepresence camera streaming and on-board physiological sensing.

Telepresence-oriented healthcare robots provide another important context because they enable remote observation and interaction in clinical or isolation-related environments. Prior telepresence and assistive-robotics studies indicate that remote presence can improve service continuity and reduce unnecessary physical contact in healthcare workflows [6], [8]. Recent telepresence-robotics reviews also show that these platforms are increasingly relevant for remote-care scenarios, but they are often designed primarily for communication, remote interaction, or clinical consultation rather than for physical delivery with embedded sensor evaluation [20]. This distinction is important because a hospital-support carrier must be evaluated not only as a communication interface, but also as a mobile robotic platform carrying loads, streaming video, and acquiring sensor data during operation.

Depth-camera-based interaction has been widely investigated for robot perception, navigation, and gesture-based control. Correa *et al.* [21] used Kinect sensing for indoor mobile-robot navigation, and Eric and Jang [22] discussed the use of Kinect depth sensing for perception support in autonomous-vehicle applications. Zhang [23] described general Kinect sensing characteristics, while healthcare-related Kinect applications have also been reviewed and explored for biomedical monitoring contexts [24], [25]. Accuracy studies further show that Kinect performance is affected by sensing range, depth accuracy, field of view, and processing conditions [26], [27], and depth-image refinement has been studied for indoor three-dimensional scene reconstruction [28]. These findings support the use of depth cameras for contactless human-robot interaction, but most prior works evaluate perception or gesture recognition as the main task rather than as an

optional human-in-the-loop control layer for a medical carrier that also performs delivery, video streaming, and vital-sign monitoring.

IoT-based physiological monitoring systems have also been developed using low-cost temperature and pulse-oximetry sensors. The MLX90614 infrared sensor has been applied for non-contact temperature measurement in practical systems [29], while IoT health-monitoring implementations have combined temperature, heart-rate, and oxygen-saturation measurements for remote observation [30], [31]. However, such systems are commonly stationary, wearable, or patient-monitoring oriented. When these sensors are embedded into a moving hospital-support robot, additional practical issues arise, including sensing distance, user positioning, Wi-Fi stability, teleoperation workflow, and the interaction between monitoring functions and payload transport.

Based on these studies, the unresolved gap is not the absence of hospital robots, telepresence systems, Kinect interfaces, or IoT vital-sign sensors as separate technologies. Rather, the gap lies in the limited experimental evaluation of a low-cost mobile carrier that integrates these capabilities into a single applied-robotics prototype. The present work therefore focuses on system-level integration and quantitative feasibility evaluation of indoor payload transport, ESP32-CAM telepresence, MLX90614/MAX30100-based monitoring, and optional Kinect-based human-in-the-loop control in one compact medical supply carrier.

3. SYSTEM DESIGN AND METHODS

Figure 1 shows the constructed prototype. The main controller is based on an ESP32 development board [32], supported by an Arduino-compatible development environment [33]. The mobile carrier chassis uses a 4WD smart car platform with motor encoders [34] driven by a motor driver module. An ESP32-CAM provides a Wi-Fi video stream using an OV2640 camera sensor [35], [36], [37]. For vital-sign monitoring, an MLX90614 infrared thermometer is employed for non-contact temperature measurement [29], and a MAX30100 module provides pulse rate and SpO2 estimation [31]. The operator accesses the mobile carrier over Wi-Fi for control and monitoring, while sensor readings are sent to the user interface.



Figure 1. Mobile carrier prototype used in experiments

3.1. Hardware architecture

The mobile carrier is built on a differential-drive base with two DC geared motors and a castor support. A lightweight multi-level frame provides separated compartments for medical supplies (*e.g.*, medicines, consumables, and small instruments) to reduce mixing and to simplify retrieval. The drive unit is powered by a rechargeable battery pack, whose practical role in sustaining mobile operation is consistent with prior characterization studies of 18650-format lithium-ion cells [38], and is controlled through an ESP32 microcontroller platform [32], which provides Wi-Fi connectivity and I/O interfaces for sensors and actuators. Motor direction and speed are generated by pulse-width modulation (PWM) control signals and applied through an H-bridge motor driver, enabling forward/backward motion and in-place turning. In addition to the drive train, the prototype integrates a temperature sensor module, a pulse-oximetry module, and a camera module, forming a single compact platform for delivery support and basic monitoring.

3.2. IoT teleoperation interface

A cloud-assisted IoT dashboard was implemented using Blynk as the user-interface layer. The dashboard provides directional buttons (forward, backward, left, right, and stop) and toggles to start/stop sensor acquisition. Commands are transmitted over Wi-Fi to the ESP32, which translates them into motor-control signals. The dashboard also displays real-time sensor values (temperature, SpO2, and pulse rate) so that an operator can monitor the device state while performing a delivery task. This approach supports rapid prototyping and can be deployed within a local hospital Wi-Fi network; in practical deployment, access control and network isolation are recommended to protect patient-related measurements. Figure 2 presents the drive chassis used as the base platform.

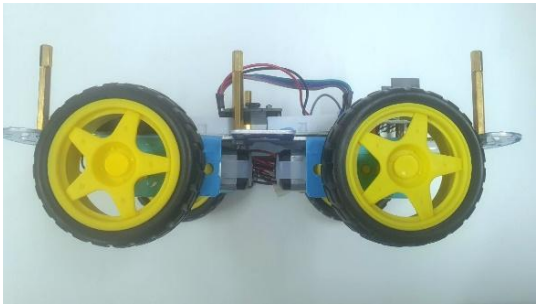

Figure 2. Differential-drive base chassis used for the mobile carrier platform

3.3. Vital-sign and temperature sensing modules

Two sensing modules were integrated for basic monitoring: i) an MLX90614 infrared thermometer for non-contact temperature measurement, and ii) a MAX30100-based pulse oximeter for estimating oxygen saturation (SpO2) and heart rate. The MLX90614 communicates via I2C and returns object temperature readings; measurements are performed without skin contact and evaluated against a commercial infrared thermometer used as a practical reference. During testing, the sensing distance was varied to characterize the effect of standoff distance on measurement error, and percentage error was calculated relative to the reference reading. The MAX30100 module also communicates via I2C and produces photoplethysmography (PPG) signals from which SpO2 and pulse rate are derived by the embedded algorithm. In this work, the MAX30100 output is treated as an estimate and compared against a commercial finger pulse oximeter as reference.

Before data recording, both sensing modules were checked for stable output at room conditions and under the intended measurement position. No post-hoc calibration correction was applied to the reported results; instead, the measured deviations are reported directly to show the practical error level of the low-cost sensing configuration. This procedure supports replicability while clarifying that the reference devices provide practical engineering benchmarks rather than clinical-grade calibration standards.

3.4. Video streaming (telepresence) module

An ESP32-CAM module with an OV2640 image sensor is used for live video streaming to the operator. The video feed supports multiple resolutions to balance clarity and bandwidth constraints (Section 5.4). In the prototype, the ESP32-CAM serves a lightweight web stream that can be accessed from a smartphone connected to the same network. This telepresence capability enables an operator to visually verify the environment and device state during delivery tasks, which is useful when direct line-of-sight monitoring is unavailable.

3.5. Gesture-based control using a depth camera (Kinect)

To provide an advanced human-in-the-loop control mode, the prototype supports gesture-based teleoperation using a depth camera (Microsoft Kinect). In this implementation, the Kinect interface functions as a supervisory control layer rather than as an autonomous navigation module. The depth stream is processed on a host computer to obtain a 3D skeletal model of the operator, from which selected joints of the right hand, left hand, head, shoulder, and spine are extracted as control features. The interface uses relative body-joint rules rather than fixed image-pixel thresholds, making the command logic easier to replicate across users with different body sizes. The overall pipeline is summarized in Figure 3.

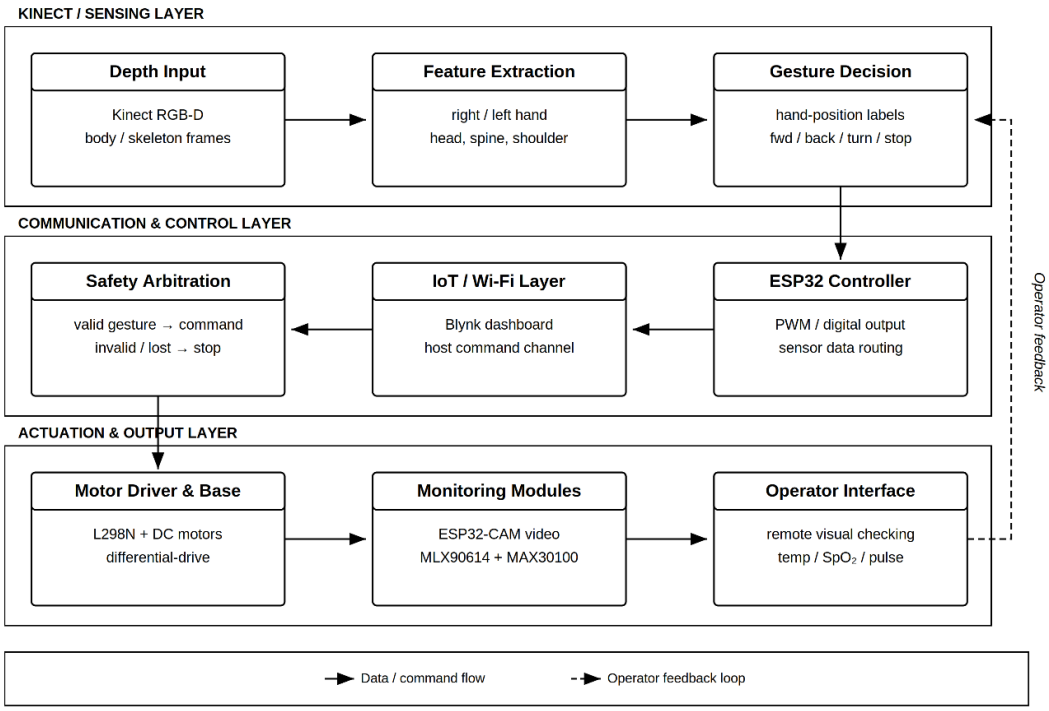

Figure 3. Kinect-based supervisory control architecture showing depth input, feature extraction, gesture decision, safety arbitration, IoT/Wi-Fi command transmission, ESP32 motor execution, monitoring modules, and operator-feedback loop

The control design uses a rule-based gesture-to-command mapping derived from relative joint positions. First, the vertical hand position is classified with respect to the head and spine midpoint; second, the horizontal hand position is classified with respect to the shoulder line; and third, the depth position is classified based on whether the hand is in front of or behind the shoulder reference. A gesture is accepted only when the required hand and body-joint coordinates are available from the Kinect skeleton stream and remain consistent with the corresponding rule during the command decision interval. These features are then mapped into five discrete motion commands: forward, backward, right turn, left turn, and stop. In the implemented mapping, both hands in the neutral-middle position indicate forward motion; the right hand in front with the left hand behind indicates backward motion; a right-side hand posture indicates right turn; a left-side hand posture indicates left turn; and both hands in the lower position indicate stop.

After a gesture is classified, the host computer transmits the corresponding command through the Wi-Fi/IoT communication layer to the ESP32 controller. The ESP32 converts the received command into motor-driver logic states for the left and right drive motors, so the high-level gesture decision is separated from the low-level actuation stage. For safety, command arbitration gives priority to stop conditions: when the gesture is not recognized, required joints are unavailable, tracking confidence decreases, the operator leaves the effective sensing range, or the input remains idle for a prolonged period, the carrier is placed in a safe-stop state while video streaming and vital-sign monitoring remain available. This rule-based safe-stop strategy provides a transparent fail-safe response without requiring probabilistic confidence tuning.

This control architecture increases the automation relevance of the prototype without claiming a new robotics algorithm. The automated part lies in the sensing-to-command pipeline, command transmission, and safety-state handling, whereas human decision-making remains in the loop for corridor navigation and obstacle awareness. The approach is therefore appropriate for an early-stage medical carrier that must remain simple, low-cost, and explainable while still supporting contactless supervisory control in infection-sensitive workflows.

4. EXPERIMENTAL SETUP

The evaluation consisted of the initial sensing, mobility, and video-streaming tests, followed by Kinect-based gesture-control evaluation and additional deployment-oriented observations. These tests included temperature measurement using MLX90614 against an infrared thermometer at multiple distances, payload-speed evaluation under incremental loading, MAX30100 vital-sign comparison, ESP32-CAM video-

streaming checks, Kinect gesture responsiveness, a 30-minute continuous-operation observation, and practical command/video latency observations. All measurements were performed in an indoor environment representative of a hospital corridor setting.

4.1. Test environment and path definition

Motion tests were performed on a flat indoor corridor-like path. The travel distance was fixed and marked on the floor to ensure repeatability. For each payload condition, the carrier was commanded to move forward along the defined path, and travel time was measured with a stopwatch; speed was computed as distance divided by time.

4.2. Temperature-sensing evaluation

The MLX90614 module was evaluated using a controlled standoff distance between the sensor and the target surface. Distances of 0.5, 1, 1.5, 2, 2.5, and 3 cm were tested to capture the effect of distance on accuracy. For each distance, the MLX90614 temperature reading was recorded and compared to a reference infrared thermometer. The absolute error and percentage error were calculated and summarized in Table 1. The temperature-measurement setup and IoT dashboard view during testing are illustrated in Figure 4.

Table 1. MLX90614 measurement vs. reference infrared thermometer at different distances

Distance (cm)	Measured temperature (°C)	Error (%)
0.5	41.21	4.59
1	39.73	0.84
1.5	37.09	5.86
2	35.07	10.99
2.5	32.97	16.32
3	30.47	22.66



Figure 4. Example of temperature measurement setup and IoT dashboard display during testing

4.3. Vital-sign evaluation

The MAX30100 module was evaluated by comparing its estimated SpO2 and pulse rate with those obtained from a commercial finger pulse oximeter. During each trial, the subject placed a finger on the MAX30100 sensor and on the reference device in a consistent manner. Readings were recorded after a short stabilization period. The purpose of this test is to quantify agreement and to identify practical limitations of low-cost pulse oximetry when integrated into a mobile platform.

4.4. Video-streaming evaluation

Video streaming was tested using several standard ESP32-CAM resolution settings. The operator accessed the stream via a smartphone on the same network and verified that it was stable. Resolution options were recorded to support implementation choices under different bandwidth constraints.

4.5. Experimental protocol and evaluation metrics

In addition, the gesture-control mode was evaluated with respect to tracking availability, gesture-sample time gap, end-to-end command latency, and successful task completion under typical indoor conditions. The initial evaluation blocks covered non-contact temperature accuracy versus a reference value using fixed sensor-object distances, pulse oximetry comparison versus a commercial oximeter across repeated trials, and mobility performance under different payload masses over a fixed path length. Additional deployment-oriented observations were then added to characterize short-duration operational stability and practical response delay under indoor Wi-Fi conditions. Where applicable, absolute error, percentage error, mean, minimum, maximum, and standard deviation were calculated. Confidence intervals are reported only

for repeated physiological measurements where the sample size supports descriptive statistical interpretation; other results are presented as engineering indicators rather than inferential clinical or certification-level tests.

4.6. Kinect-based gesture-control evaluation

A basic evaluation was conducted to characterize the feasible operating range and sampling responsiveness of the Kinect-based gesture interface. The operator stood at predefined distances (60-480 cm) from the sensor and performed the supported gestures used for teleoperation. Tracking success was recorded as detected/undetected at each distance; intermittent detection was noted when the skeleton or gesture signal became unstable. To approximate responsiveness, the time gap between consecutive tracked gesture samples was computed from recorded timestamps. Because the Kinect stream is processed on the host computer, the measured gaps may vary with CPU/GPU load, lighting, partial occlusion, user posture, and acquisition settings.

5. RESULTS AND DISCUSSION

5.1. Temperature sensing (MLX90614)

Table 1 summarizes the MLX90614 temperature readings at different sensing distances. The data show a clear distance-dependent trend: the lowest error is obtained at 1 cm (0.84%), while the error increases progressively as the sensor is moved farther away and reaches 22.66% at 3 cm. This decrease in accuracy is expected for low-cost infrared thermometry because increasing standoff distance enlarges the effective spot area, increases sensitivity to target nonuniformity, and allows more ambient background influence to enter the measurement. For the proposed mobile carrier, these results imply that the temperature module is suitable for short-range screening support, but only when the user or robot positions the sensor at a controlled distance.

For engineering deployment, the result suggests that the temperature module should be used with a fixed short-range measurement procedure rather than a free-distance measurement. A simple mechanical positioning guide, offset calibration at the selected distance, repeated sampling, and moving-average filtering should be implemented before broader deployment. If the measured distance is uncertain or the target is outside the recommended range, the dashboard should warn the operator to reposition the sensor instead of reporting the value as reliable.

Figure 5 visualizes the distance-dependent error trend as a scatter plot with a fitted quadratic curve ($y = 3.69x^2 - 4.81x + 4.63$), where each data point represents a single measurement at the corresponding sensor-object distance. The curve is used as a visual guide rather than as a physical sensor model. The observed minimum error at 1 cm indicates the best tested distance for the current prototype setup, while the sharp increase beyond 2 cm shows that uncontrolled hand placement or changing target distance can dominate the temperature error. The physical measurement setup corresponding to this fixed-distance MLX90614 evaluation is shown in Figure 6.

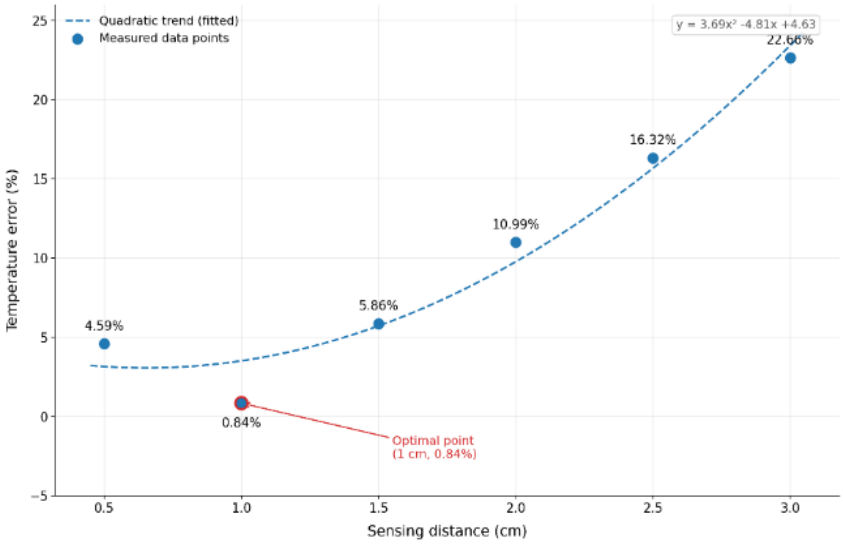

Figure 5. Distance-dependent MLX90614 temperature-error trend showing the need for fixed short-range positioning in the sensing workflow, which is essential for reliable non-contact screening in mobile hospital-logistics robot deployment



Figure 6. Temperature measurement setup using MLX90614

5.2. Payload-speed evaluation

Table 2 reports the travel time and derived speed for each payload level tested. As shown in Figure 7, the measured data points reveal a clear monotonic degradation in mobility as payload increases: speed decreases from 0.375 m/s at 0.278 kg to 0.091 m/s at 2.098 kg, and the prototype can no longer complete the motion test at 2.445 kg. Linear regression over the seven successful payload points yields an approximate slope of −0.15 m/s per kg, confirming a consistent and progressive degradation of speed with added load. This pattern indicates that the useful payload boundary is governed by drivetrain torque margin and wheel-floor interaction rather than by tray volume alone. For hospital workflow planning, the carrier should therefore be assigned to light-duty delivery tasks and should not be operated near the stall threshold.

Table 2. Payload–speed results for the mobile carrier over a fixed-distance path

Load condition	Load size	Mass (kg)	Path length (m)	Travel time (s)	Speed (m/s)
1 boxed milk carton	250 ml	0.278	3	8	0.375
2 boxed milk cartons	500 ml	0.556	3	9	0.333
3 boxed milk cartons	750 ml	0.833	3	11	0.273
3 boxed milk cartons + 1 small mineral-water bottle	750 ml + 330 ml	1.180	3	11	0.273
3 boxed milk cartons + 2 small mineral-water bottles	750 ml + 660 ml	1.527	3	16	0.188
3 boxed milk cartons + 1 large mineral-water bottle + 1 small mineral-water bottle	750 ml + 600 ml + 330 ml	1.813	3	21	0.143
3 boxed milk cartons + 2 large mineral-water bottles	750 ml + 600 ml + 600 ml	2.098	3	33	0.091
3 boxed milk cartons + 2 large mineral-water bottles + 1 small mineral-water bottle	750 ml + 600 ml + 600 ml + 330 ml	2.445	3	—	—

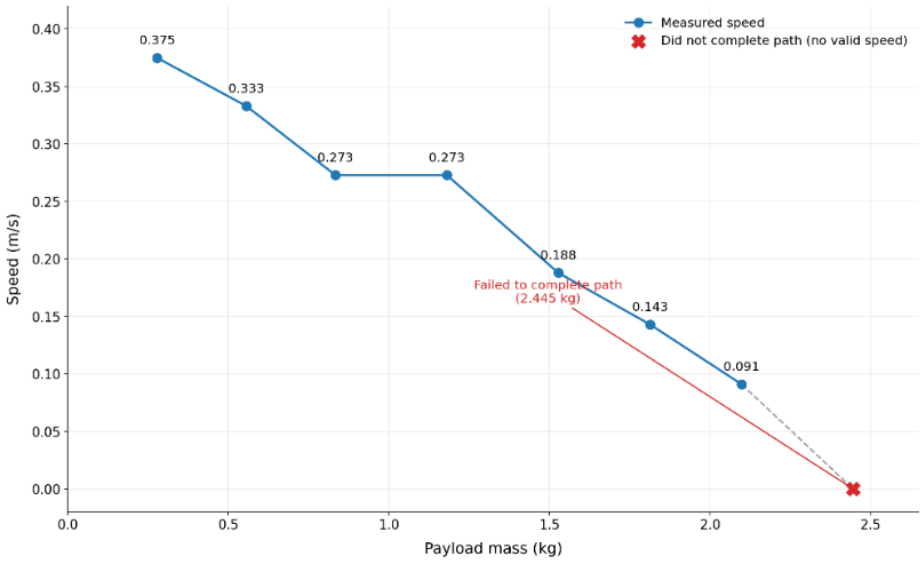

Figure 7. Payload-speed degradation curve identifying the mobile carrier operating envelope and failed payload condition, indicating the drivetrain constraint that governs light-duty robot deployment for hospital logistics

Although motor current and detailed battery discharge were not measured in the present prototype, the payload-speed trend in Figure 7 provides an indirect engineering indicator of drivetrain operating margin. The steep speed reduction near the maximum successful payload suggests that additional load produces rapidly increasing mechanical and electrical demand. Future drivetrain characterization should therefore include motor voltage/current logging, battery state-of-charge estimation, wheel-slip observation, and repeated duty-cycle testing so that payload capacity can be specified from measured powertrain performance rather than from single-pass mobility alone.

5.3. Vital-sign monitoring (MAX30100)

A sample vital-sign measurement and dashboard readout are shown in Figure 8, while the module used during testing is shown in Figure 9. Table 3 summarizes the comparison between the MAX30100 module and a commercial finger pulse oximeter. Across 10 trials, the SpO2 error was relatively small, with a mean of 1.13% and standard deviation of 0.75% (approximate 95% confidence interval: 0.67-1.60%). Pulse-rate error was higher, with a mean of 6.92% and standard deviation of 5.66% (approximate 95% confidence interval: 3.41-10.42%). These values indicate that SpO2 estimation was more stable than pulse-rate estimation in the current low-cost setup.



Figure 8. MAX30100 vital-sign measurement example showing sensor placement, reference pulse oximeter comparison, and IoT dashboard readout



Figure 9. MAX30100 pulse-oximetry module integrated as a low-cost supportive monitoring sensor

Table 3. MAX30100 measurement vs. commercial pulse oximeter (SpO2 and pulse rate)

No	SpO2 ref (%)	Pulse ref (bpm)	SpO2 MAX30100 (%)	Pulse MAX30100 (bpm)	Error SpO2 (%)	Error pulse (%)
1	98	76	96	74.82	2.04%	1.55%
2	95	80	96	72.65	1.05%	9.19%
3	95	81	96	84.88	1.05%	4.79%
4	96	77	96	82.53	0.00%	7.18%
5	97	78	96	91.91	1.03%	17.83%
6	95	86	96	73.52	1.05%	14.51%
7	96	76	96	75.76	0.00%	0.32%
8	97	76	96	77.96	1.03%	2.58%
9	98	79	96	76.02	2.04%	3.77%
10	98	77	96	82.73	2.04%	7.44%
			Average error		1.13%	6.92%

The larger pulse-rate error can be attributed to the sensitivity of PPG signals to finger pressure, slight motion, local perfusion, sensor placement, and the embedded low-cost algorithm. Therefore, the MAX30100 should be interpreted as a supportive monitoring module for trend observation rather than a clinical diagnostic instrument. To improve measurement reliability, future implementation should add a stabilization period, repeated sampling, median or moving-average filtering, a simple finger-placement guide, and outlier rejection before values are displayed or logged.

5.4. Video streaming resolution

Table 4 lists the tested video-streaming resolutions for the ESP32-CAM module. Rather than treating these options merely as image formats, they represent a design trade-off between situational awareness, bandwidth demand, latency, and processing load. Lower resolutions such as quarter video graphics array (QVGA) are more suitable for responsive teleoperation under constrained Wi-Fi conditions, whereas higher resolutions may provide better visual detail but require stronger network and browser performance.

Table 4. ESP32-CAM video streaming resolution options used in testing

Category	Resolution (pixels)
QVGA	320 × 240
VGA	640 × 480
SVGA	800 × 600
XGA	1024 × 768
HD	1280 × 720
UXGA	1600 × 1200

The current video test confirms functional streaming at selectable resolutions and is complemented by the preliminary practical latency observations. However, these observations do not replace a full network-quality analysis. Future work should include controlled measurements of frame rate, end-to-end video latency, packet loss, reconnection time, and the effect of multiple simultaneous devices on the same hospital Wi-Fi network.

5.5. Comparison with related works

To position the proposed prototype within the context of recent service-robot and hospital delivery platforms, Table 5 provides a functional comparison with representative related systems. The comparison emphasizes not only delivery or teleoperation capability, but also telepresence, embedded sensing, supervisory control, and deployment implications. This framing highlights the robotics and automation contribution of the work: the prototype is evaluated as an integrated system rather than as a single-purpose transport cart or standalone monitoring unit.

Table 5. Functional comparison with representative hospital service-robot studies

Work	Primary function	Control/automation mode	Telepresence and sensing	Deployment gap in prior work	Contribution/implication
[11]	Patient assistance robot	Remote/assistance-oriented operation	Telepresence or physiological sensing not central	Focuses on assistance; limited integration of delivery, video, and vital monitoring	Shows need for broader healthcare-support integration
[14]	Hospital AGV logistics	Path-following/guided mobility	Patient-parameter monitoring is limited; no gesture interface	Requires prepared paths and has limited flexible human-in-the-loop supervision	Motivates supervised mobile carrier for dynamic corridor use
[17]	IoT patient-service robot	IoT-enabled remote operation	Video/IoT support without integrated vital-sign evaluation	System integration is shown but experimental sensing and telepresence evaluation are limited	Supports IoT-based service robotics context
[19]	Service robots for infection reduction	Deployment-oriented service robotics	Focus on infection-risk reduction rather than module-level sensing	Does not quantify integrated payload, monitoring, and control performance	Provides workflow relevance for contact-reduction logistics
This work	Medical supply carrier with monitoring	IoT teleoperation plus Kinect-based supervisory control and safe-stop behavior	ESP32-CAM video, MLX90614 temperature, MAX30100 SpO2/pulse, and payload transport	Current prototype still requires longer-duration endurance, detailed battery profiling, and broader network validation	Demonstrates a low-cost integrated baseline for scalable healthcare robotics deployment

Overall, the experimental results indicate that the prototype is technically feasible for low-load indoor assistance tasks, while also making its present limitations explicit. The mobility tests show that payload capacity is constrained primarily by the drivetrain, the sensing tests show that measurement quality depends strongly on operating conditions, and the streaming tests highlight the dependence of telepresence quality on network availability. Compared with hospital service-robot studies that focus mainly on delivery assistance or hospital-support logistics [11], [14], [17], [19], this work demonstrates a broader functional scope by combining transport, monitoring, and remote visual supervision in one platform. The main implication is not that the prototype is ready for autonomous deployment, but that it provides a practical and measurable baseline for further robotics development in low-cost healthcare-support scenarios.

In a practical hospital workflow, the carrier can be interpreted as a supervised automation aid between a nurse station, corridor path, and patient-room handover point. The operator remains responsible for motion decisions, while the platform automates repetitive command execution, remote observation, and basic sensor readout. This division of responsibility is appropriate for an early-stage healthcare-support robot

because it reduces unnecessary physical movement without claiming full autonomy or unsupervised clinical deployment.

5.6. Gesture-based control evaluation (Kinect)

To substantiate the gesture-based control mode, we report a Kinect tracking-range test and a response proxy (average time gap between consecutive tracked gesture samples). Table 6 shows that reliable tracking is achieved between 120-420 cm, while 450 cm becomes intermittent and 480 cm is not detected. Table 7 summarizes measured time gaps of 49-187 ms across the detected distances. These values are acceptable for human-in-the-loop teleoperation, where the operator remains in the control loop and can tolerate moderate latency, but they also indicate that the interaction performance is distance- and computation-dependent rather than uniform across the workspace. In practical corridor operation, the results suggest that Kinect-based control is feasible when the user stands within a moderate range, line-of-sight is maintained, and host-processing load is controlled.

Table 6. Kinect gesture tracking performance versus user distance

User–Kinect distance (cm)	Gesture tracked?
60	Yes (neck-down); upper-neck not detected (outside camera FOV)
120	Yes
180	Yes
240	Yes
300	Yes
420	Yes
450	Intermittent
480	No

Table 7. Measured the Kinect gesture-sample time gap versus user distance

User–Kinect distance (cm)	Avg. time gap between consecutive tracked data (ms)
60	141
120	49
180	187
240	153
300	128
420	161
450	N/A
480	N/A

These results support the inclusion of gesture-based control as an additional interaction layer for safe, hands-free operation in clinical corridors. From a robotics standpoint, the Kinect module is not intended to replace autonomous navigation; instead, it complements teleoperation by offering a contactless supervisory interface that can be useful in infection-sensitive or hands-busy environments. The safe-stop behavior under reduced tracking confidence is also important because it links perception reliability directly to motion safety.

Related studies on body-based gesture interpretation [39], Kinect posture and tracking accuracy [40], Kinect-controlled ground vehicles [41], practical ESP32 integration [42], gesture-based mobile-robot control [43], distance measurement using Kinect [44], smoothing of Kinect body joints for kinematic analysis [45], Kinect v2 joint and coordinate interpretation [46], experimental evaluation of Kinect accuracy and capture rate for rehabilitation-oriented motion tracking [47], recent gesture-command-based teleoperation for multiple robots [48], and recent studies on mitigating teleoperation delays through perception-oriented system design [49] provide relevant context for these observations. In comparison with those studies, the present work applies depth-camera interaction in a narrower but practical setting: command issuance for a medical-support carrier with simultaneous monitoring and video streaming. This applied integration perspective is the main contribution of the Kinect module in the present paper.

From an automation perspective, the gesture interface contributes a supervisory control layer rather than a fully autonomous controller. Its reliability should therefore be evaluated in future work through repeated start-stop cycles, command success rate, tracking-loss frequency, and recovery time after safe-stop events. Such metrics would directly address long-term usability and safety in realistic corridor operation.

5.7. Engineering implications for automation, scalability, and deployment

The proposed platform can be scaled by treating the carrier as a modular mechatronic unit: the mobile base, ESP32 controller, ESP32-CAM, MLX90614, MAX30100, Kinect interface, and dashboard layer can each be upgraded or replaced without changing the overall workflow. This modularity is relevant to manufacturing and deployment because it supports repeatable assembly, maintenance, and subsystem testing before hospital use.

For broader automation, the present architecture provides a transition path from supervised teleoperation to semi-automated logistics. The current system already supports remote command execution, visual telepresence, sensor readout, gesture-based command generation, and safe-stop behavior. Future industrialized versions should add standardized enclosures, cable protection, battery-management

monitoring, access control, audit logging, and validation of continuous operation under repeated delivery cycles.

The results also indicate that hospital deployment should be planned as a workflow integration problem rather than only as a robot-design problem. The carrier should be matched to light-load tasks, short-range sensor measurement procedures, defined Wi-Fi coverage zones, and operator training for gesture or dashboard control. These considerations connect the prototype to healthcare automation and manufacturing-system readiness while keeping the present claims within the experimentally validated operating envelope.

5.8. Additional deployment-oriented validation

To address deployment-oriented requirements for reliability, latency, and practical automation, two additional validation checks were conducted after the initial prototype evaluation. The first check observed short-duration continuous operation under repeated teleoperation commands while video streaming and sensor readout remained active. The second check estimated practical command and video latency under indoor Wi-Fi conditions using repeated trials and visual observation from recorded tests. These checks extend the prototype evaluation toward deployment readiness while remaining within the feasibility-level scope of the study.

Table 8 summarizes the results of the 30-minute continuous-operation observation. Across the monitored metrics, the prototype demonstrated stable behavior during the session. All 50 repeated command cycles-comprising forward, stop, right turn, left turn, and backward sequences-were executed without command failure, indicating that the ESP32-based control loop and Wi-Fi command channel remained usable under sustained teleoperation load. The web dashboard remained responsive, the video stream showed no visible interruption, and sensor readouts remained available during the test. No controller reset was observed, and no excessive heating was identified after the session, with only slight warmth observed in the motor driver and motors. Battery voltage decreased from 12.6 to 11.9 V over 30 min, indicating measurable energy use under combined motion, streaming, and sensing tasks; however, a formal runtime claim requires longer endurance testing with current and voltage logging.

Table 8. Continuous-operation and reliability observation under repeated teleoperation, video streaming, and sensor-readout tasks

Metric	Observation condition	Result/observation
Test duration	30 min continuous operation	Completed successfully without system freeze or connection drop.
Operation mode	Repeated teleoperation commands with video streaming and sensor reading active	Teleoperation, video streaming, and sensor readout ran concurrently; the web dashboard remained responsive.
Number of repeated command cycles	Forward-stop-right turn-stop-left turn-stop-backward-stop	50 complete cycles were executed without command failure.
Controller reset	Observed during the test	0 resets; the ESP32 controller operated stably throughout the session.
Video-stream interruption	Observed during the test	No visible interruption was observed; the stream remained usable for remote supervision.
Sensor-readout interruption	MLX90614 and MAX30100 readout availability	No interruption was observed; sensor readouts remained available on the dashboard.
Command failure	Number of commands not executed during the repeated cycles	0 command failures; all repeated commands produced visible carrier responses.
Observed overheating	Motor driver, motor, battery, or controller condition after the test	No excessive heating was observed; components were only slightly warm after the test.
Battery-voltage observation	Initial and final battery voltage	Initial: 12.6 V; final: 11.9 V; no sudden voltage drop was observed.

Table 9 summarizes the latency observations obtained using a software-based timestamping approach, and Figure 10 visualizes the mean delay and observed range for each tested command or video-stream condition. For command-response latency (dashboard and Kinect), the delay was measured as the elapsed time between a logged command-dispatch event on the host side and the first visible carrier motion detected from a co-recorded video, with timestamps extracted frame-by-frame at 30 fps (approximately 33 ms resolution). For video-stream latency, a stopwatch displayed simultaneously on the host monitor and within the ESP32-CAM frame was compared across synchronized screenshots, yielding an approximate one-way stream delay. Dashboard command response averaged 65 ms, Kinect gesture-command response averaged 88 ms, QVGA video streaming averaged 125 ms, and VGA video streaming averaged 168 ms. The higher video-stream latency at VGA confirms the expected resolution-bandwidth trade-off and supports the use of lower resolution when responsiveness is prioritized.

Table 9. Practical command and video latency observation under indoor Wi-Fi operation

Test item	No. of trials	Mean delay	Minimum delay	Maximum delay	Observation
Dashboard command response	10	65 ms	49 ms	85 ms	Delay from button press to visible carrier response.
Kinect gesture-command response	10	88 ms	72 ms	110 ms	Delay from gesture decision to visible carrier response.
ESP32-CAM video stream at QVGA	5	125 ms	112 ms	145 ms	Approximate delay using stopwatch-display comparison.
ESP32-CAM video stream at VGA	5	168 ms	150 ms	187 ms	Approximate delay using stopwatch-display comparison.

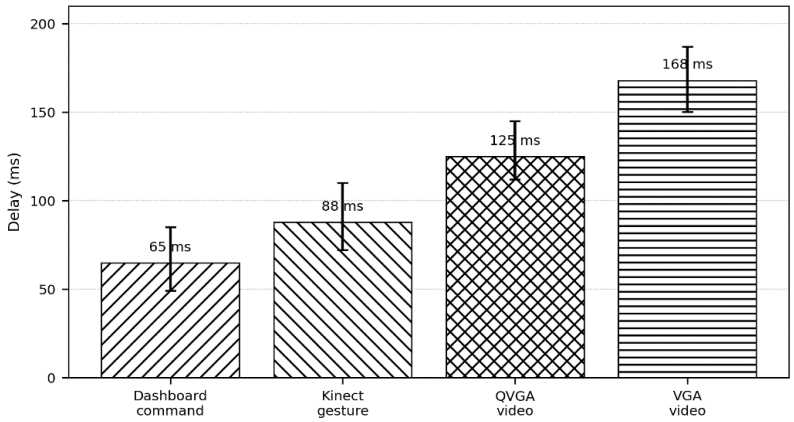

Figure 10. Patterned bar chart of practical command and video latency observations, showing the delay increase from dashboard and Kinect commands to QVGA and VGA video streaming

These latency values should not be interpreted as deterministic real-time control guarantees. Under real hospital conditions, measured latency may increase due to router load from concurrent devices, RF interference from medical equipment, ESP32-CAM thermal throttling during extended sessions, browser rendering overhead on lower-spec operator terminals, and host-computer CPU load from co-running applications. The software-based timestamping method used here also introduces a frame-level measurement uncertainty of approximately one video frame (≈33 ms), which should be accounted for when comparing these results with benchmarks obtained by hardware-instrumented latency analyzers or network packet-capture tools.

For future work, latency characterization should be repeated using hardware-instrumented methods—such as network packet capture with precision timestamps or dedicated latency-measurement firmware—to obtain resolution below 1 ms and to separate network propagation delay from ESP32-CAM encoding latency and host-side rendering delay. Testing under variable Wi-Fi load and at greater distances from the access point is also recommended to characterize latency degradation under realistic hospital network conditions.

6. LIMITATIONS AND FUTURE WORK

6.1. Practical implications and limitations

The results indicate that the proposed system is feasible as a proof-of-concept teleoperated medical carrier, but they also define a clear practical operating envelope. MLX90614 accuracy deteriorates rapidly outside a short sensing distance, meaning that temperature measurement requires deliberate positioning by the operator or robot. The MAX30100 module provides useful physiological trends, yet its pulse-rate variability indicates that low-cost PPG sensing should be treated as supportive monitoring rather than clinical diagnosis. Mobility performance is strongly payload-dependent; once the carried mass approaches the drivetrain limit, speed decreases substantially and task completion becomes unreliable. Together, these findings show that the prototype is suitable for light-duty indoor assistance and telepresence-oriented workflows, but not yet for heavy-duty or fully autonomous hospital logistics.

Some reviewer-suggested evaluations were not claimed as completed in this study because the current prototype was not instrumented for formal drivetrain-efficiency measurement, detailed battery-discharge

profiling, clinical-grade sensor validation, or safety/regulatory certification. These items are therefore treated as limitations of the present proof-of-concept scope and as future engineering validation tasks rather than as completed results. A future version should integrate current and voltage sensing, battery-state monitoring, duty-cycle endurance testing, latency logging, emergency-stop validation, speed limiting, cybersecurity assessment, cleaning/disinfection procedures, and institutional safety review before hospital deployment.

In particular, drivetrain efficiency should be evaluated using measured motor voltage/current and payload-dependent speed, while battery endurance should be evaluated through controlled discharge tests under idle, streaming, sensing, and motion modes. Safety and regulatory readiness should be assessed through risk analysis, fail-safe testing, operator-training procedures, and documentation for hospital workflow integration. These future evaluations are outside the scope of the present revision but are explicitly identified to guide the next prototype iteration.

Several limitations follow from this proof-of-concept scope. First, the study uses a single prototype, so manufacturing repeatability, unit-to-unit variability, and long-term durability are not yet established. Second, the mobility function is based on human teleoperation, and autonomous path planning, obstacle avoidance, localization, and multi-floor deployment are outside the present implementation. Third, payload tests were limited to short indoor trajectories. Although the additional 30-min operation check provides an initial reliability observation, long-term endurance, battery lifetime, motor-current behavior, and drivetrain durability were not fully characterized. Fourth, the practical latency observations were obtained under one indoor Wi-Fi condition using visual estimation, so they do not replace formal network-quality measurements such as packet loss, automated end-to-end timestamp logging, frame-rate stability, and reconnection time. Fifth, the sensing modules are low-cost components benchmarked against practical reference devices rather than clinically validated instruments. These limitations should be understood as boundaries of the current prototype rather than weaknesses of the proposed integration concept.

Future work should therefore prioritize improvements that directly strengthen the robotics value of the platform: a more robust mechanical and powertrain design for higher payload stability, safer motion control with emergency-stop and speed-limiting strategies, stronger cybersecurity and access control for networked monitoring, and the gradual addition of navigation intelligence such as waypoint following, obstacle-aware assistance, and multi-floor hospital workflow testing. On the sensing side, calibration, filtering, signal-conditioning, and operator-guided measurement procedures are needed before broader deployment-oriented studies can be justified.

6.2. Gesture-based (Kinect) control: limitations and future directions

Beyond autonomous waypoint following, the gesture-based control mode provides a practical human-in-the-loop option for constrained indoor situations such as narrow corridors, temporary obstacles, or crowded zones where manual intent can be safer and faster than replanning. By using a depth camera for skeletal tracking, the operator can issue commands hands-free while the system maintains continuous video streaming and vital-sign monitoring. The experimental results show that this interaction mode is usable only within a bounded operating range, so workspace positioning and line-of-sight management remain important implementation considerations.

From an engineering perspective, the key design benefit is the separation between i) perception and gesture inference at the interface layer and ii) motion execution at the embedded controller. This separation enables a safety-first arbitration policy: when tracking confidence decreases because of occlusion, out-of-range positioning, or computation limits, the carrier can default to a safe-stop state. Future work can extend this framework with richer gesture vocabularies, sensor fusion between depth and other perception modalities, and more systematic evaluation of latency, workload, and task success rate under realistic lighting and corridor conditions.

7. CONCLUSION

This paper presented and evaluated a low-cost IoT-enabled mobile medical supply carrier as an applied robotics prototype for indoor healthcare-support logistics. The system integrates payload transport, non-contact temperature sensing, pulse-oximetry monitoring, real-time video streaming, and an optional Kinect-based human-in-the-loop gesture interface in a single mobile platform. The results define a realistic operating envelope: the MLX90614 sensor achieved its lowest temperature error at 1 cm (0.84%) and showed increasing error up to 22.66% at 3 cm; the carrier completed payload trials up to 2.098 kg with reduced speed (0.091 m/s), while motion failed at 2.445 kg; the MAX30100 yielded average errors of 1.13% for SpO2 and 6.92% for pulse rate; and Kinect tracking was reliable at 120-420 cm with gesture-sample gaps of 49-187 ms. Additional validation showed stable 30-min operation over 50 command cycles and practical command-response latency below 110 ms for dashboard and Kinect command modes.

The main contribution of this work is not a new autonomous-navigation algorithm, but proof-of-concept validation and system-level integration of logistics mobility, telepresence, embedded physiological sensing, and gesture-based supervisory control on one compact low-cost platform. This integration is practically significant for healthcare workflows that require light-duty delivery, remote observation, and supportive patient-condition sensing under supervised operation. The current prototype remains limited by payload capacity, short-range temperature-sensing requirements, low-cost pulse-oximetry variability, single-prototype testing, absence of motor-current monitoring, and limited controlled indoor validation. Future work should prioritize autonomous or waypoint-assisted navigation, calibrated sensing and error compensation, sensor filtering, stronger drivetrain and power design, cybersecurity mechanisms, safety validation, automated latency and reliability logging, and testing in realistic hospital environments.

ACKNOWLEDGMENTS

The authors would like to thank LPPM Universitas Trisakti for the PIPP research grant support, and Centre for Artificial Intelligence and Advanced Technology (CAPTIVATE) for the collaboration and technical assistance during prototyping and evaluation. The prototype concept described in this work is associated with an Indonesian granted simple patent, No. IDS000012710, application No. S00202512957, entitled "*Sistem troli medis otomatis dengan kendali jarak jauh menggunakan gerakan tubuh*." The authors used ChatGPT as an editorial assistance tool for language refinement and revision organization. The authors remain fully responsible for the scientific content, data, references, analysis, and conclusions of this manuscript.

FUNDING INFORMATION

This work was supported by the PIPP research grant from LPPM Universitas Trisakti.

AUTHOR CONTRIBUTIONS STATEMENT

This journal uses the Contributor Roles Taxonomy (CRediT) to recognize individual author contributions, reduce authorship disputes, and facilitate collaboration.

Name of Author	C	M	So	Va	Fo	I	R	D	O	E	Vi	Su	P	Fu
Henry Candra	✓	✓	✓	✓	✓				✓	✓		✓	✓	✓
Umi Yuniati				✓		✓	✓	✓		✓				
Tjhwa Endang Djuana		✓		✓						✓		✓		
Indra Surjati		✓		✓			✓			✓		✓		
Raden Deiny Mardian Wijayapraja			✓	✓		✓		✓		✓				
Syah Alam			✓	✓		✓	✓	✓						
Yuli Kurnia Ningsih							✓					✓	✓	
Lydia Sari							✓			✓	✓			
Rifai Chai	✓	✓								✓		✓		
Angellia Lestari Candra										✓	✓		✓	

C : **C**onceptualization
M : **M**ethodology
So : **So**ftware
Va : **Va**lidation
Fo : **Fo**rmal analysis
I : **I**nvestigation
R : **R**esources
D : **D**ata Curation
O : Writing - **O**riginal Draft
E : Writing - Review & **E**diting
Vi : **Vi**sualization
Su : **Su**pervision
P : **P**roject administration
Fu : **Fu**nding acquisition

CONFLICT OF INTEREST STATEMENT

The authors declare that they have no conflict of interest.

DATA AVAILABILITY

The authors confirm that the data supporting the findings of this study are available within the article.

REFERENCES

[1] A. A. Morgan, J. Abdi, M. A. Q. Syed, G. El Kohen, P. Barlow, and M. P. Vizcaychipi, "Robots in healthcare: a scoping review," *Current Robotics Reports*, vol. 3, no. 4, pp. 271–280, 2022, doi: 10.1007/s43154-022-00095-4.

[2] D. Silvera-Tawil, "Robotics in healthcare: A survey," *SN Computer Science*, vol. 5, no. 1, 2024, doi: 10.1007/s42979-023-02551-0.

[3] R. Wang *et al.*, "A medical assistive robot for telehealth care during the COVID-19 pandemic: development and usability study in an isolation ward," *JMIR Human Factors*, vol. 10, 2023, doi: 10.2196/42870.

[4] N. C. Tan *et al.*, "Introducing a healthcare-assistive robot in primary care: a preliminary questionnaire survey," *Frontiers in Robotics and AI*, vol. 10, p. 1123153, 2023, doi: 10.3389/frobt.2023.1123153.

[5] J. Laigaard, T. U. Fredskild, and G. L. Fojecki, "Telepresence robots at the urology and emergency department: A pilot study assessing patients' and healthcare workers' satisfaction," *International Journal of Telemedicine and Applications*, vol. 2022, p. 8787882, 2022, doi: 10.1155/2022/8787882.

[6] A. Altalbe, M. N. Khan, M. Tahir, and A. Shahzad, "Orientation control design of a telepresence robot: An experimental verification in healthcare system," *Applied Sciences (Switzerland)*, vol. 13, no. 11, p. 6827, 2023, doi: 10.3390/app13116827.

[7] G. D'Onofrio and D. Sancarlo, "Assistive robots for healthcare and human–robot interaction," *Sensors*, vol. 23, no. 4, p. 1883, 2023, doi: 10.3390/s23041883.

[8] L. Almeida, P. Menezes, and J. Dias, "Telepresence social robotics towards co-presence: A review," *Applied Sciences (Switzerland)*, vol. 12, no. 11, p. 5557, 2022, doi: 10.3390/app12115557.

[9] L. Chen, C. Li, A. Fahmy, and J. Sienz, "GestureMoRo: an algorithm for autonomous mobile robot teleoperation based on gesture recognition," *Scientific Reports*, vol. 14, no. 1, p. 6199, 2024, doi: 10.1038/s41598-024-54488-w.

[10] H. Esaki and K. Sekiyama, "Immersive robot teleoperation based on user gestures in mixed reality space," *Sensors*, vol. 24, no. 15, p. 5073, 2024, doi: 10.3390/s24155073.

[11] B. S. Pranathi, A. Nair, C. S. Anushree, and T. S. Chandar, "Sahayantra - a patient assistance robot," in *2020 11th International Conference on Computing, Communication and Networking Technologies, ICCCNT 2020*, 2020, pp. 1–6. doi: 10.1109/ICCCNT49239.2020.9225444.

[12] I. Haider, K. B. Khan, M. A. Haider, A. Saeed, and K. Nisar, "Automated robotic system for assistance of isolated patients of coronavirus (COVID-19)," *Proceedings - 2020 23rd IEEE International Multi-Topic Conference, INMIC 2020*. IEEE, pp. 1–6, 2020. doi: 10.1109/INMIC50486.2020.9318124.

[13] M. F. Hasan, I. Rahaman, M. S. Sayem, M. M. Hasan, B. K. Tamal, and M. A. R. Rubel, "Designing of cost-effective human assistive robot and performance enhancement," *2020 11th International Conference on Computing, Communication and Networking Technologies, ICCCNT 2020*. IEEE, pp. 1–5, 2020. doi: 10.1109/ICCCNT49239.2020.9225599.

[14] M. Antony, M. Parameswaran, N. Mathew, S. V.S, J. Joseph, and C. M. Jacob, "Design and implementation of automatic guided vehicle for hospital application," *2020 5th International Conference on Communication and Electronics Systems (ICCES)*. IEEE, pp. 1031–1036, 2020. doi: 10.1109/icces48766.2020.9137867.

[15] J. C. Chien, Z. Y. Dang, and J. Der Lee, "Navigating a service robot for indoor complex environments," *Applied Sciences (Switzerland)*, vol. 9, no. 3, p. 491, 2019, doi: 10.3390/app9030491.

[16] K. L. Narayanan *et al.*, "Fuzzy guided autonomous nursing robot through wireless beacon network," *Multimedia Tools and Applications*, vol. 81, no. 3, pp. 3297–3325, 2022, doi: 10.1007/s11042-021-11264-6.

[17] J. F. Rusdi, A. Nurhayati, H. Gusdevi, M. I. Fathulloh, A. Priyono, and R. Hardi, "IoT-based Covid-19 patient service robot design," *3rd International Conference on Cybernetics and Intelligent Systems, ICORIS 2021*. IEEE, pp. 1–6, 2021. doi: 10.1109/ICORIS52787.2021.9649461.

[18] S. Vongbunyong, S. P. Tripathi, K. Thamrongaphichartkul, N. Worrasittichai, A. Takutruea, and T. Prayongrak, "Simulation of autonomous mobile robot system for food delivery in in-patient ward with Unity," *Proceedings - 2020 15th International Joint Symposium on Artificial Intelligence and Natural Language Processing, iSAI-NLP 2020*. IEEE, pp. 1–6, 2020. doi: 10.1109/iSAI-NLP51646.2020.9376784.

[19] H. Dadi, M. Al-Haidous, N. Radwi, and L. Ismail, "Service robots in hospitals to reduce spreading of COVID-19," in *2021 Fifth World Conference on Smart Trends in Systems Security and Sustainability (WorldS4)*, Jul. 2021, vol. 14, no. 2, pp. 212–217. doi: 10.1109/WorldS451998.2021.9514018.

[20] K. Youssef, S. Said, S. Al Kork, and T. Beyrouthy, "Telepresence in the recent literature with a focus on robotic platforms, applications and challenges," *Robotics*, vol. 12, no. 4, p. 111, 2023, doi: 10.3390/robotics12040111.

[21] D. S. O. Correa, D. F. Sciotti, M. G. Prado, D. O. Sales, D. F. Wolf, and F. S. Osório, "Mobile robots navigation in indoor environments using Kinect sensor," *Proceedings - 2012 2nd Brazilian Conference on Critical Embedded Systems, CBSEC 2012*. pp. 36–41, 2012. doi: 10.1109/CBSEC.2012.18.

[22] N. Eric and J. W. Jang, "Kinect depth sensor for computer vision applications in autonomous vehicles," in *International Conference on Ubiquitous and Future Networks, ICUFN*, Jul. 2017, pp. 531–535. doi: 10.1109/ICUFN.2017.7993842.

[23] Z. Zhang, "Microsoft kinect sensor and its effect," *IEEE Multimedia*, vol. 19, no. 2, pp. 4–10, 2012, doi: 10.1109/MMUL.2012.24.

[24] H. Candra, U. Yuniati, and R. Chai, "The application of virtual reality using Kinect sensor in biomedical and healthcare environment: A review," in *Lecture Notes in Electrical Engineering*, vol. 1182, Springer Nature Singapore, 2024, pp. 15–38. doi: 10.1007/978-981-97-1463-6_2.

[25] A. Al-Naji, K. Gibson, S. H. Lee, and J. Chahl, "Real time apnoea monitoring of children using the microsoft kinect sensor: A pilot study," *Sensors (Switzerland)*, vol. 17, no. 2, p. 286, 2017, doi: 10.3390/s17020286.

[26] L. Yang, L. Zhang, H. Dong, A. Alelaiwi, and A. El Saddik, "Evaluating and improving the depth accuracy of Kinect for Windows v2," *IEEE Sensors Journal*, vol. 15, no. 8, pp. 4275–4285, 2015, doi: 10.1109/JSEN.2015.2416651.

[27] O. Wasenmüller and D. Stricker, "Comparison of kinect v1 and v2 depth images in terms of accuracy and precision," in *Lecture Notes in Computer Science*, vol. 10117 LNCS, 2017, pp. 34–45. doi: 10.1007/978-3-319-54427-4_3.

[28] J. Jiao, L. Yuan, W. Tang, Z. Deng, and Q. Wu, "A post-rectification approach of depth images of Kinect v2 for 3D reconstruction of indoor scenes," *ISPRS International Journal of Geo-Information*, vol. 6, no. 11, p. 349, 2017, doi: 10.3390/ijgi6110349.

[29] A. Sudianto, Z. Jamaludin, A. A. Abdul Rahman, S. Novianto, and F. Muharrom, "Smart temperature measurement system for milling process application based on MLX90614 infrared thermometer sensor with Arduino," *Journal of Advanced Research in Applied Mechanics*, vol. 72, no. 1, pp. 10–24, 2020, doi: 10.37934/aram.72.1.1024.

[30] A. N. Costrada, A. G. Arifah, I. D. Putri, I. K. A. Sara Sawita, H. Harmadi, and M. Djamal, "Design of heart rate, oxygen saturation, and temperature monitoring system for Covid-19 patient based on Internet of Things (IoT)," *Jurnal Ilmu Fisika |*

Universitas Andalas, vol. 14, no. 1. pp. 54–63, 2022. doi: 10.25077/jif.14.1.54-63.2022.
[31] A. D. (Maxim Integrated), "MAX30100: Pulse oximeter and heart-rate sensor IC for wearable health, data sheet (Rev. 0)," *Analog*. Sep. 2014. Accessed: Jan. 12, 2026. [Online]. Available: https://www.analog.com/media/en/technical-documentation/data-sheets/max30100.pdf
[32] Espressif Systems, "ESP32 — esp-dev-kits documentation." https://docs.espressif.com/projects/esp-dev-kits/en/latest/esp32/index.html (accessed Jan. 12, 2026).
[33] "Overview of the Arduino IDE 1," *docs.arduino.cc*. 2025. Accessed: Jan. 12, 2026. [Online]. Available: https://docs.arduino.cc/software/ide-v1/tutorials/Environment
[34] "4WD robot smart car chassis kit with speed encoder," *Maker Store*. 2026. Accessed: Jan. 12, 2026. [Online]. Available: https://www.makerstore.com.au/product/robo-4wdsmartcar-chassis-kit/
[35] SunFounder, "GalaxyRVR Mars Rover kit for Arduino Uno R3 (ESP32 CAM)," *SunFounder*. 2025. Accessed: Jan. 12, 2026. [Online]. Available: https://www.sunfounder.com/products/sunfounder-galaxyrvr-mars-rover-kit
[36] Arducam, "OV2640: Specs, Datasheet \& Alternatives." Accessed: Jan. 12, 2026. [Online]. Available: https://blog.arducam.com/ov2640/
[37] "OV2640 CameraChip™ Color CMOS UXGA (2.0 Megapixel) Sensor: Preliminary Datasheet," *OMNIVISION TECHNOLOGIES*. 2006. Accessed: Jan. 12, 2026. [Online]. Available: https://www.uctronics.com/download/cam_module/OV2640DS.pdf
[38] V. Muenzel *et al.*, "A comparative testing study of commercial 18650-format lithium-ion battery cells," *Journal of The Electrochemical Society*, vol. 162, no. 8, pp. A1592--A1600, 2015, doi: 10.1149/2.0721508jes.
[39] M. Ousmer, J. Vanderdonckt, and S. Buraga, "An ontology for reasoning on body-based gestures," in *Proceedings of the ACM SIGCHI Symposium on Engineering Interactive Computing Systems, EICS 2019*, Jun. 2019, pp. 1–6. doi: 10.1145/3319499.3328238.
[40] P. Abbondanza, S. Giancola, R. Sala, and M. Tarabini, "Accuracy of the microsoft kinect system in the identification of the body posture," in *Lecture Notes of the Institute for Computer Sciences, Social-Informatics and Telecommunications Engineering, LNICST*, vol. 192, 2017, pp. 289–296. doi: 10.1007/978-3-319-58877-3_37.
[41] S. Amir, A. Waqar, M. A. Siddiqui, M. Majeed, H. Haseeb, and S. H. Mehmood, "Kinect controlled UGV," *Wireless Personal Communications*, vol. 95, no. 2, pp. 631–640, Jul. 2017, doi: 10.1007/s11277-016-3915-3.
[42] R. Mischianti, "DOIT ESP32 DEV KIT v1: high resolution pinout and specs - Mischianti," *Mischianti Blog*. 2025. Accessed: Jan. 12, 2026. [Online]. Available: https://mischianti.org/doit-esp32-dev-kit-v1-high-resolution-pinout-and-specs/
[43] K. Cekova, N. Koceska, and S. Koceski, "Gesture control of a mobile robot using Kinect sensor," in *Proceedings of ICAIIT2016*, Jun. 2016, pp. 251–258. doi: 10.20544/aiit2016.31.
[44] Vangos Pterneas, "Measuring distances using Kinect – The right way," *Pterneas*. Aug. 2016. Accessed: Jan. 12, 2026. [Online]. Available: https://pterneas.com/2016/08/11/measuring-distances-kinect/
[45] N. K. Mangal and A. K. Tiwari, "Kinect v2 tracked body joint smoothing for kinematic analysis in musculoskeletal disorders," in *Proceedings of the Annual International Conference of the IEEE Engineering in Medicine and Biology Society, EMBS*, 2020, vol. 2020-July, pp. 5769–5772. doi: 10.1109/EMBC44109.2020.9175492.
[46] Lisa Jamhoury, "Understanding Kinect V2 joints and coordinate system," *Medium*. pp. 1–7, Jul. 2018. Accessed: Jan. 12, 2026. [Online]. Available: https://lisajamhoury.medium.com/understanding-kinect-v2-joints-and-coordinate-system-4f4b90b9df16
[47] D. Webster and O. Celik, "Experimental evaluation of Microsoft Kinect's accuracy and capture rate for stroke rehabilitation applications," in *IEEE Haptics Symposium, HAPTICS*, Feb. 2014, pp. 455–460. doi: 10.1109/HAPTICS.2014.6775498.
[48] L. A. Zick, D. Martinelli, A. Schneider de Oliveira, and V. Cremer Kalempa, "Teleoperation system for multiple robots with intuitive hand recognition interface," *Scientific Reports*, vol. 14, no. 1, p. 30230, 2024, doi: 10.1038/s41598-024-80898-x.
[49] J. Du, W. Vann, T. Zhou, Y. Ye, and Q. Zhu, "Sensory manipulation as a countermeasure to robot teleoperation delays: system and evidence," *Scientific Reports*, vol. 14, no. 1, p. 4333, 2024, doi: 10.1038/s41598-024-54734-1.

BIOGRAPHIES OF AUTHORS



Henry Candra is a Ph.D. graduate from the University of Technology Sydney and a lecturer at Universitas Trisakti since 1997. His research specializes in biomedical engineering and smart systems, focusing on the development of IoT-enabled mobile medical supply carriers that integrate real-time vital-sign monitoring and video streaming to optimize remote healthcare logistics. He can be contacted at henrycandra@trisakti.ac.id.



Umi Yuniati is a graduate of electrical engineering from Universitas Trisakti, Indonesia, and currently works as a Patent Examiner at the Directorate General of Intellectual Property of Indonesia. She handles patent applications in electrical engineering and telecommunications, as well as integrated-circuit layout designs. Her research interests include information and communication technology, healthcare technology, biomedical systems, and virtual reality. She can be contacted at 162012200005@std.trisakti.ac.id or yuniati.umi@gmail.com.



Tjhwa Endang Djuana is a lecturer in Department of Electrical Engineering, Faculty of Industrial Technology, Universitas Trisakti Jakarta Indonesia. He received the Bachelor of Engineering (S.T.) degree in electrical engineering majoring in control system engineering from Universitas Trisakti, Jakarta, Indonesia, in 1996. He received the Master of Engineering (M.Eng.) degree in information technology from the Royal Melbourne Institute of Technology (RMIT) University, Melbourne, Australia, in 2000. He finishes his Ph.D. study majoring in data science (Computer Science) at the Queensland University of Technology (QUT), Brisbane, Australia, in 2016. He has served in various role in the Department, as Secretary and Head of Department and currently serves as Head of Control System Laboratory. He has also coordinated the Renewable Energy and Artificial Learning Machine (REALM) research group, the Digital Acceleration Center (DAC) and Center of Excellence in Artificial Intelligence and Advanced Technology (CAPTIVATE). He can be contacted at edjuana@trisakti.ac.id.



Indra Surjati is a professor at the Professional Program for Engineers, Faculty of Industrial Technology, Universitas Trisakti, Jakarta, Indonesia, specializing in electrical engineering with extensive research expertise in wireless communication systems and antenna technology. Her work in optimizing radio frequency engineering and high-speed data transmission is foundational to the development of reliable IoT frameworks, particularly for systems requiring stable connectivity for real-time monitoring and mobile data streaming. As a prolific researcher and IEEE member, she focuses on advancing the wireless infrastructure necessary to support integrated smart technologies and mobile healthcare solutions. She can be contacted at indra@trisakti.ac.id.



Raden Deiny Mardian Wijayapraja was born in Medan, Indonesia. He received the Bachelor of Engineering (S.T.) degree in electrical engineering from Universitas Trisakti in 1998. He then obtained his Master of Engineering (M.T.) degree, also in electrical engineering, from Universitas Trisakti in 2001. He earned his Doctoral (Dr.) degree in electrical engineering from Universitas Indonesia in 2022, with a focus on quality of experience (QoE) measurement models for video streaming services in 5G technology. Currently, he serves as the Secretary of the Department and a Senior Lecturer in the Department of Electrical Engineering, Universitas Trisakti. His research interests include telecommunications, digital broadcasting, wireless communications, and QoS/QoE analysis. He can be contacted at deiny_wp@trisakti.ac.id.



Syah Alam was born in Jakarta, Indonesia. He received the Bachelor of Education (S.Pd.) degree in electrical engineering from the Universitas Pendidikan Indonesia (UPI), in 2010, the M.Eng (M.T.) degree in telecommunication engineering from the Graduate Program of Electrical Engineering, Universitas Trisakti, in 2012, and the Ph.D. degree in electronic engineering (RF and microwave) from the Universiti Teknikal Melaka Malaysia (UTeM), in 2024. In 2018, he joined the Department of Electrical Engineering, Universitas Trisakti, as a Researcher and a Lecturer. Since 2023, he has been appointed as associate professor in microwave technology in the Electrical Engineering Study Program, Universitas Trisakti. His research interests include microstrip antenna and microwave sensors for various applications. He can be contacted at syah.alam@trisakti.ac.id.



Yuli Kurnia Ningsih is a lecturer at Universitas Trisakti, Indonesia. She has extensive experience in academic management, having served as Vice Dean of the Faculty of Industrial Technology (2011–2021) and Secretary of the Master's Program in electrical engineering. She is currently Secretary of the Professional Engineer Program and Director of PT LAT, an affiliated institution of the Faculty of Industrial Technology. Her research interests include wireless communication, antenna systems, the Internet of Things (IoT), and vehicular communication, with publications in several journals, including the Eastern-European Journal of Enterprise Technologies. Her academic contributions include curriculum development, quality improvement in higher education, and active involvement in research and innovation supporting industrial technology. She can be contacted at yuli_kn@trisakti.ac.id.



Lydia Sari is an associate professor in the Department of Electrical Engineering at Universitas Trisakti, Indonesia. Her research focuses on information theory, with particular emphasis on data compression and error-correcting codes, wireless communication systems, and communication security. She has authored and co-authored numerous scholarly publications and is actively engaged in research and academic activities aimed at advancing communication engineering and higher education. She can be contacted at lydia_sari@trisakti.ac.id.



Rifai Chai is an associate professor and academic director (Partnerships) at the School of Engineering, Swinburne University of Technology. His research focuses on biomedical engineering and artificial intelligence, particularly brain–body applications, embedded systems, and the design of biomedical devices. He has industry experience in hardware/firmware/software product development in Indonesia and Australia (2000–2011). His research interests include embedded systems, AI/ML, brain–computer interfaces, medical technologies, robotics and autonomous systems, and assistive technologies. He can be contacted at rchai@swin.edu.au.



Angellia Lestari Candra is with the Electrical Engineering Department, Faculty of Industrial Technology, Universitas Trisakti, Jakarta, Indonesia. Her research interests include IoT, embedded systems, and applied robotics. She can be contacted at 062002300001@std.trisakti.ac.id.